Evolution of Ferrofluid Droplet Deformation Under Magnetic Field in a Uniaxial Flow

Debdeep Bhattacharjee, Arnab Atta, and Suman Chakraborty

Abbreviations

Nomenclature

Bo_m	Magnetic Bond number
Cn	Cahn number
Ca	Capillary number
λ	Viscosity ratio
M	Mason number
μ_r	Relative magnetic permeability
Re	Reynolds number

Subscripts

i	Droplet phase
e	Suspending medium

D. Bhattacharjee (✉) · A. Atta
Department of Chemical Engineering, IIT Kharagpur, Kharagpur, West Bengal 721302, India
e-mail: debdeepbhattacharjee@ymail.com

S. Chakraborty
Department of Mechanical Engineering, IIT Kharagpur, Kharagpur, West Bengal 721302, India

K. M. Singh et al. (eds.), *Fluid Mechanics and Fluid Power, Volume 5*, Lecture Notes in Mechanical Engineering, https://doi.org/10.1007/978-981-99-6074-3_42

1 Introduction

Immense industrial and biomedical applications (e.g., polymer processing, magnetically controlled optics, ferrofluid-based sensors, biomedical imaging, drug delivery, and diagnosis of malignant tumors) make the droplet magnetohydrodynamics an emerging area of research for the last few decades [1–5].

In the case of the flow field, the droplet deformation depends on the nondimensional capillary number (Ca), which signifies the ratio between viscous force (that tries the droplet to deform) and the interfacial force (that maintains the droplet to its initial spherical shape). Following the pioneering research (on the droplet dynamics of Newtonian fluid under the governance of background flow in a small deformation regime) of Taylor [6], Han and Chin [7] experimented to show the deformation and breakup characteristics of the droplet in extensional flow. Here they considered both the droplet phase and continuous phase to be viscoelastic and showed the effects of different fluid properties (such as viscosity, elasticity, and interfacial tension) on the deformation dynamics. Moreover, droplet breakups in linear flows have been adequately examined numerically as well as experimentally by Stone [8]. Furthermore, Delaby et al. [9] experimentally exhibited the importance of the viscosity ratio on the deformation dynamics of a droplet in immiscible molten polymer blends for higher Ca limits. Minale [10] analytically shows the droplet deformation considering (i) both the phases are Newtonian, (ii) one of the phases is non-Newtonian, and (iii) considering the confined system where wall effects have been considered.

Similarly, the sole impact of a uniform magnetic field on the ferro-droplet has been thoroughly addressed in the literature [11–13]. On a brief note, the appearance of a magnetic field makes the ferro-droplet unstable and expands along with the applied magnetic field orientation [14]. In this context, Afkhami et al. [12, 13] analytically showed the dependency of the aspect ratio (ratio between the length of major and minor axes) of the deformed droplet on the magneto-physical properties of the ferrofluid. A complete numerical study on hysteresis phenomena for the ferro-droplet deformation in a uniform magnetic field has been studied by Lavrova et al. [15].

The dynamics of a neutrally buoyant droplet in the presence of the magnetic field or extensional flow are independently reported in the literature. The droplet dynamics in the combined effect of magnetic field and uniaxial extensional flow can provide many physical imaginations on the fluid mixing controllability. Motivated by this, here we propose to see the impact of the uniform magnetic field in the background uniaxial extensional flow on the ferro-droplet dynamics. Considering Stokes flow, the magnetohydrodynamic problem is solved by following numerical simulations in the small deformation limit.

2 Problem Formulation

Here, we considered a Newtonian ferrofluid droplet of radius r_i, density ρ, viscosity η_i, and magnetic susceptibility χ_i, placed in another Newtonian, non-magnetic fluid of viscosity η_e and density ρ (neutrally buoyant) as shown in Fig. 1. The droplet is directed by an externally employed magnetic field $\overline{\boldsymbol{H}}_0 = H_0 \boldsymbol{e}_z$ and uniaxial extensional flow $\overline{\boldsymbol{U}}_0 = \overline{\mathbf{T}}_0 \cdot \overline{\boldsymbol{X}}$. Here, H_0 is the magnitude of the applied magnetic field, $\overline{\mathbf{T}}_0$ is the rate of the strain tensor, and $\overline{\boldsymbol{X}}$ is the position vector. The far-field strain rate tensor $\overline{\mathbf{T}}_0$ can be defined as:

$$\overline{\boldsymbol{T}}_0 = \frac{G_0}{2}\begin{bmatrix} -1 & 0 & 0 \\ 0 & -1 & 0 \\ 0 & 0 & 2 \end{bmatrix} \tag{1}$$

where G_0 is the rate of strain. Further, we considered the surface tension σ is uniform along with the droplet interface.

2.1 Governing Equations

The velocity field for an incompressible flow satisfies the continuity and Navier–Stokes equation as [16, 17]:

$$\left.\begin{aligned} \nabla \cdot \mathbf{u} &= 0 \\ \rho\left(\frac{\partial \mathbf{u}}{\partial t} + \mathbf{u}\,\nabla\,\mathbf{u}\right) &= -\nabla p + \eta\,\nabla \cdot \left(\nabla \mathbf{u} + (\nabla \mathbf{u})^{\boldsymbol{T}}\right) + \mathbf{F}_{\mathrm{ST}} + \mathbf{F}_{\mathrm{M}} \end{aligned}\right\} \tag{2}$$

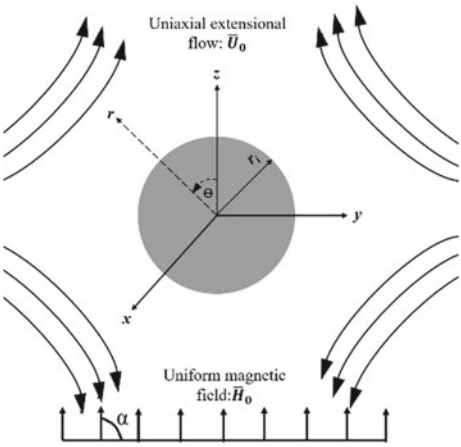

Fig. 1 Schematic representation of the problem description

Here $\mathbf{F}_{\mathrm{ST}}$ and $\mathbf{F}_{\mathrm{M}}$ represent the force due to surface tension and magnetic force, respectively. The surface tension force, $\mathbf{F}_{\mathrm{ST}}$ can be described as [18]:

$$\mathbf{F}_{\mathrm{ST}} = \nabla \cdot \left[\sigma \mathbf{I} + \left(-\mathbf{n}\mathbf{n}^{T}\right)\delta\right] \tag{3}$$

where $\mathbf{I}$, δ, and $\mathbf{n}$ are the second-order identity tensor, Dirac delta function, and unit normal to the interface. Similarly, the force due to magnetic field, $\mathbf{F}_{\mathrm{M}}$ can be defined as [18]:

$$\mathbf{F}_{\mathrm{M}} = \nabla \cdot \boldsymbol{\tau}_{\mathrm{M}} = \nabla \cdot \left(\mu_m \mathbf{H}\mathbf{H}^{\mathrm{T}} - \frac{\mu_m}{2}(\mathbf{H} \cdot \mathbf{H})\mathbf{I}\right) \tag{4}$$

In the above equation, $\mathbf{H}$, $\boldsymbol{\tau}_{\mathrm{M}}$, and μ_m are the strength of the applied magnetic field, magnetic stress tensor, and the magnetic permeability of the fluid, respectively. To find the magnetic stress tensor, we need to solve the magneto-static Maxwell equations as given below [18].

$$\left.\begin{aligned} \nabla \cdot \mathbf{B} &= 0 \\ \nabla \times \mathbf{H} &= 0 \\ \mathbf{M} &= \chi_m \mathbf{H} \\ \mathbf{B} &= \mu_0(\mathbf{H} + \mathbf{M}) \end{aligned}\right\} \tag{5}$$

where μ_0 ($\mu_0 = 4\pi \times 10^{-7}$ N/A^2) is the permeability of the vacuum. $\mathbf{B}$, $\mathbf{M}$, and χ_m are magnetic induction, magnetization, and magnetic susceptibility, respectively.

2.2 *Nondimensionalization*

To nondimensionalize, we have considered the following scales: length—r_i, velocity—$G_0 r_i$, magnetic field strength—H_0, hydrodynamic stress—$\eta_e G_0$, and magnetic stress—$\mu_0 {H_0}^2$. Here we assumed that the viscous force is ruling over the inertia force, resulting in a low Reynolds number flow. We have tabulated all the dimensionless parameters and nondimensional numbers in Table 1.

3 Numerical Method

In this study, we used the phase-field technique to resolve the two-phase interface features. Phase-field model for a system of two incompressible and immiscible fluids can be described as [19]:

$$\frac{\partial \psi(x,t)}{\partial t} + \mathbf{u} \cdot \nabla \psi(x,t) = \nabla\left(M_{\psi(x,t)} \nabla G\right) \tag{6}$$

Table 1 Different dimensionless parameters and nondimensional numbers associated with the present analysis

Symbol	Details
λ	Viscosity ratio defined as $\lambda = \eta_i/\eta_e$
μ_r	Relative magnetic permeability defined as $\mu_{r,i} = \mu_i/\mu_0$ (droplet phase) (we have considered the suspending medium as non-magnetic in this study, i.e., $\mu_{r,e} = \mu_e/\mu_0 = 1$)
Re	Reynolds number defined as $\mathrm{Re} = \rho G_0 r_i^2/\eta_e$ (ratio between inertial and viscous stress)
Ca	Capillary number defined as $\mathrm{Ca} = \eta_e G_0 r_i/\sigma$ (magnitude of viscous stress relative to capillary stress)
Bo_m	Magnetic Bond number defined as $\mathrm{Bo}_m = r_i \mu_0 \lvert\mathbf{H}_0\rvert^2/\sigma$ (magnitude of magnetic stress relative to capillary stress)
M	Mason number defined as $M = \mu_0 \lvert\mathbf{H}_0\rvert^2/\eta_e G_0$ (magnitude of magnetic stress relative to viscous stress)

where $M_{\psi(x,t)}$ and G denote the interface mobility factor and chemical potential, respectively. Two fluids are distinguished by the definite values of the phase-field parameter $\psi(x,t)$. The values of the phase-field parameter for suspending fluid phase and droplet phase are taken as -1 and $+1$, respectively; whereas it varies from -1 to $+1$ at the two-phase interface.

The magnetic potential follows Poisson's equation in the following form [18]:

$$\nabla \cdot \left(\mu_m \nabla \phi^{mag}\right) = 0 \tag{7}$$

where μ_m is the magnetic permeability of the fluid which can be presented in terms of the phase-field parameter as

$$\mu_m = \left[\frac{(1+\psi(x,t))}{2}\mu_i\right] + \left[\frac{(1-\psi(x,t))}{2}\mu_e\right] \tag{8}$$

For simulations, a square channel of size $L \times L$ is considered (here $L = 10r_i$ to neglect the effect of channel confinement), where the droplet is situated at the center of the left side (axis of symmetry) as shown in Fig. 2.

3.1 Grid Independence and Cahn Number Independence Test

To check the precision of the simulation results, the grid independence and Cahn number (Cn) independence assessments are necessary. In our model, the grid size and the Cahn number are similar and close to the two-phase interface. So, an accurate grid independence study automatically confirms a correct Cahn number independence analysis [20]. For the Cahn number independence study, we have compared the

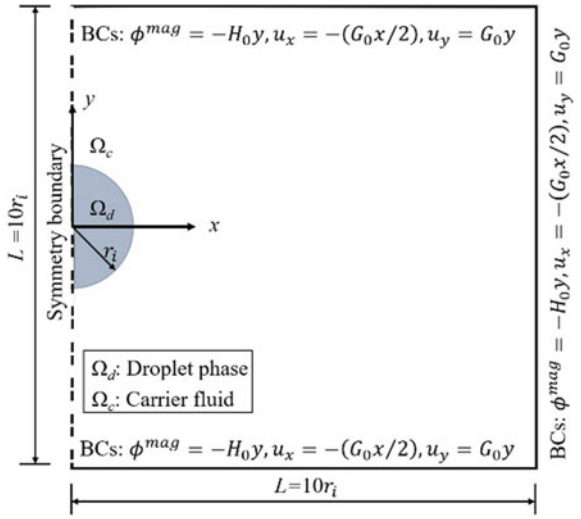

Fig. 2 Schematic representation of the computational domain

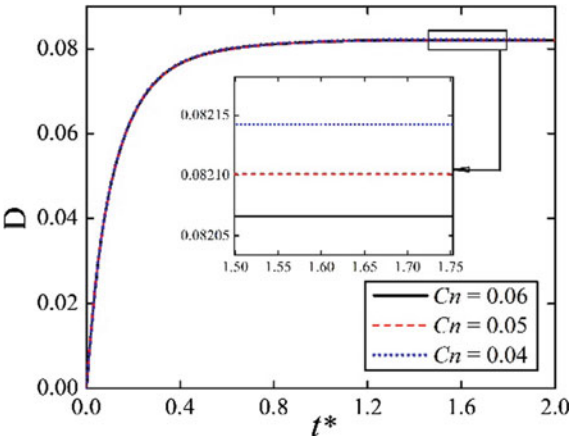

Fig. 3 Alteration of the droplet deformation for different Cahn numbers (Cn) at Ca = 0.05, λ = 1 in the sole presence of uniaxial extensional flow

temporal droplet deformation in presence of uniaxial flow as illustrated in Fig. 3. This figure confirms that the droplet deformation is almost the same for three different values of the Cahn number. Eventually, we considered $Cn = 0.04$ for the rest of our analysis.

3.2 Model Validation

For validation, we have compared the deformation parameter D [where $D = (l - b)/(l + b)$; l and b are the lengths of the major and minor axis of the deformed droplet,

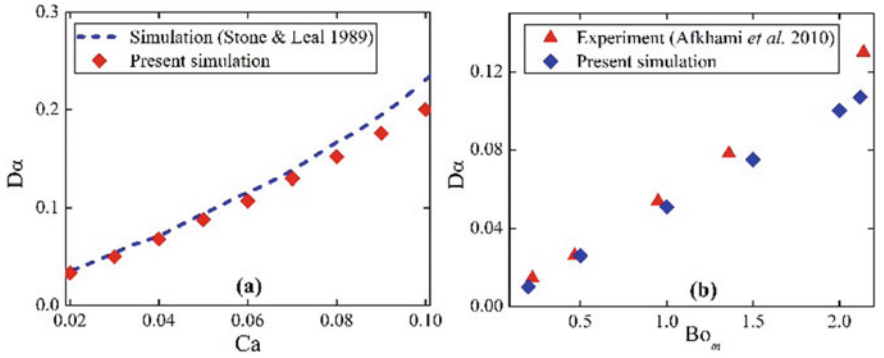

Fig. 4 Alteration of the droplet deformation at the steady-state (D_α) with **a** Capillary number Ca at $\lambda = 1$ in uniaxial extensional flow and **b** Magnetic Bond number Bo_m for $(\mu_{r,i}, \mu_{r,e}) = (1.89, 1)$ in sole existence of uniform magnetic field

respectively] with the previously reported results for two cases: (a) droplet deformation in existence of uniaxial extensional flow only and (b) droplet deformation in the sole presence of the uniform magnetic field. Figure 4a shows the steady-state droplet deformation (D_α) for different Ca values at $\lambda = 1$, which confirms that our numerical model is in harmony with the simulation of Stone and Leal [21]. Figure 4b depicts the alteration of droplet deformation at the steady-state (D_α) with the magnetic Bond number (Bo_m) for $\mu_{r,i} = 1.89$. After comparison, we found that our numerical model is in the same fashion as the experimental results of Afkhami et al. [13] for $Bo_m < 1.5$.

4 Results and Discussion

In external flow conditions, the viscosity ratio plays a pivotal role in the deformation dynamics of a droplet. Figure 5 confirmed the impact of the viscosity ratio on the droplet deformation in the Stokes flow regime (here, $Re = 0.01$). It can be seen that at a fixed Ca value (here, $Ca = 0.05$), as the viscosity ratio (λ) increases from 0.01 to 5, the deformation parameter (D) also increases. Contrariwise, the time taken to reach steady-state deformation is smaller at the lower viscosity ratio. Another important observation is that for $\lambda \leqslant 1$, the temporal evolution of the droplet deformation is almost independent of the viscosity ratio. More precisely, the droplet deformation plot at $\lambda = 0.01$ almost coincides with that at $\lambda = 0.1$. Considering these aspects, we considered $\lambda = 1$ to see the droplet deformation characteristics for the rest of the analysis.

Figure 6a illustrates the transient droplet deformation for $(\mu_{r,i}, \mu_{r,e}) = (2, 1)$ and $\lambda = 1$ for different Mason numbers and $\alpha = 90°$. In absence of a magnetic field (i.e., $M = 0$), the drop deforms into a prolate shape due to the hydrodynamic stress

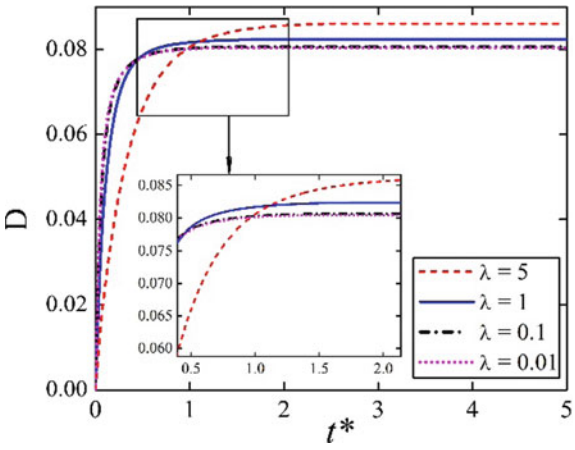

Fig. 5 Effect of viscosity ratio (λ) on the droplet deformation (D) for Ca = 0.05, $M = 0$, and Re = 0.01

distribution. For all $M > 0$ at $\alpha = 90°$, both the magnetic stress and the hydrodynamic stress are acting in the same direction which assists the droplet to deform into a prolate shape. Moreover, the deformation increases with increasing magnetic field strength. Figure 6b depicts the alteration of transient deformation of the ferro-droplet for $(\mu_{r,i}, \mu_{r,e}) = (2, 1)$ and $\lambda = 1$ with different Mason numbers at $\alpha = 0°$. Here the magnetic stress tries to resist the prolate deformation aided by hydrodynamic stress. For this reason, the deformation for all $M > 0$ is less when compared with $M = 0$. Fascinatingly, here we observed two distinct droplet shape deformations. For $M =$ 0, 1, and 5, it forms a prolate shape, whereas, for higher values of M (= 10, 20), it deforms into an oblate shape. The prolate shape formation is because of the higher viscous force compared with the magnetic force. While, for $M = 10$ and 20, the magnetic stress becomes relatively high so that it overcomes the viscous force and deformed the droplet into an oblate shape.

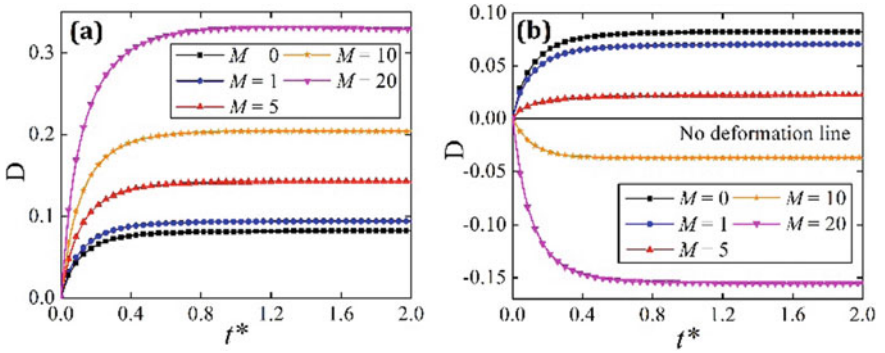

Fig. 6 Alteration of droplet deformation (D) with time for $(\mu_{r,i}, \mu_{r,e}) = (2, 1)$ and $\lambda = 1$ for different Mason numbers. **a** $\alpha = 90°$and **b** $\alpha = 0°$. Other parameters are Ca = 0.05 and Re = 0.01

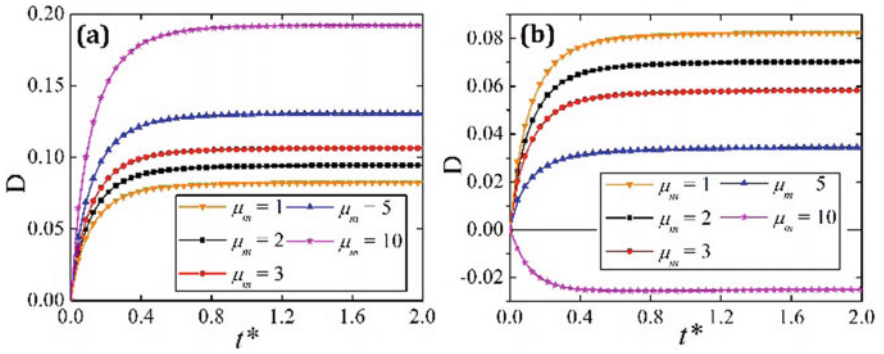

Fig. 7 Alteration of droplet deformation (D) with time for different relative magnetic permeability of the droplet phase ($\mu_{r,i}$) for **a** $(M, \alpha) = (1, 90°)$ and **b** $(M, \alpha) = (1, 0°)$. Other parameters are $\mu_{r,e} = 1$, Ca = 0.05, $\lambda = 1$, and Re = 0.01

The relative magnetic permeability of a material represents the ability of that material to be magnetized in presence of an external magnetic field. The magnetic force exerted on a ferrofluid droplet directly depends on its relative magnetic permeability. Hence, the relative magnetic permeability has a key role in droplet morphology alteration. Figure 7a represents that for a system with $\alpha = 90°$, the droplet deformation (D) increases monotonically with the relative magnetic permeability at a fixed magnetic field strength. This observation follows a similar trend as reported in the literature [22]. This is because the magnetic stress attributed to the droplet pole increases with an increase in relative magnetic permeability. Consequently, the magnetic force dominates the surface tension force and thus the droplet becomes more elongated along the direction of the magnetic field and forms a prolate shape with a high aspect ratio. Interestingly, for the system $(M, \alpha) = (1, 0°)$ as shown in Fig. 7b, the droplet morphology evolved from prolate to oblate shape with the increase of relative magnetic permeability from 1 to 10. This is because with the increase of $\mu_{r,i}$, the magnetic stress becomes high and it governs the flow dynamics. As a result, the droplet follows the magnetic field direction and formed an oblate shape.

5 Conclusions

In summary, the transient dynamics of a ferro-droplet guided by the uniform magnetic field in background uniaxial extensional flow has been studied numerically. Based on the outcomes, the major findings are as follows:

- The droplet deforms into a prolate shape for $\alpha = 90°$. On the contrary, for $\alpha = 0°$, the droplet may deform into either a prolate or oblate shape depending on the Mason number.

- For the system with $\alpha = 90°$, the droplet elongates more with the higher relative magnetic permeability and forms the prolate shape. Whereas, an enhancement of relative magnetic permeability can change the droplet morphology from the prolate to an oblate shape at $\alpha = 0°$.

Acknowledgements D.B. thanks Dr. Somnath Santra for his insight on numerical analyses. S.C. acknowledges the Sir J. C. Bose National Fellowship awarded by the DST, Government of India.

References

1. Garstecki P, Stone HA, Whitesides GM (2005) Mecism for flow-rate controlled breakup in confined geometries: a route to monodisperse emulsions. Phys Rev Lett 94(16):164501
2. Dutz S, Clement JH, Eberbeck D, Gelbrich T, Hergt R, Muller R, Wotschadlo J, Zeisberger M (2009) Ferrofluids of magnetic multicore nanoparticles for biomedical applications. J Magn Magn Mater 321(10):1501–1504
3. Torres-D´ıaz I, Rinaldi C (2014) Recent progress in ferrofluids research: novel applications of magnetically controllable and tunable fluids. Soft Matter **10**(43):8584–8602
4. McClements DJ (2015) Emulsion stability, food emulsions. CRC Press, pp 314–407
5. Bhattacharjee D, Atta A, Chakraborty S (2022) Magnetic field altered ferrofluid droplet deformation in the uniaxial extensional flow. B Am Phys Soc
6. Taylor GI (1932) The viscosity of a fluid containing small drops of another fluid. Proc R Soc Lond Ser A 138(834):41–48
7. Chin BH, Han DC (1979) Studies on droplet deformation and breakup. I. Droplet deformation in extensional flow. J Rheol 23(5):557–590
8. Stone HA (1994) Dynamics of drop deformation and breakup in viscous fluids. Annu Rev Fluid Mech 26(1):65–102
9. Delaby I, Ernst B, Germain Y, Muller R (1994) Droplet deformation in polymer blends during uniaxial elongational flow: Influence of viscosity ratio for large capillary numbers. J Rheol 38(6):1705–1720
10. Minale M (2010) Models for the deformation of a single ellipsoidal drop: a review. Rheol Acta 49(8):789–806
11. Rosensweig RE (1985) Ferrohydrodynamics. Cambridge University Press
12. Afkhami S, Renardy Y, Renardy M, Riffle JS, St Pierre T (2008) Field-induced motion of ferrofluid droplets through immiscible viscous media. J Fluid Mech 610:363–380
13. Afkhami S, Tyler AJ, Renardy Y, Renardy M, St Pierre TG, Woodward RC, Riffle JS (2010) Deformation of a hydrophobic ferrofluid droplet suspended in a viscous medium under uniform magnetic fields. J Fluid Mech 663:358–384
14. Liu J, Yap YF, Nguyen NT (2011) Numerical study of the formation process of ferrofluid droplets. Phys Fluids 23(7):072008
15. Lavrova O, Polevikov V, Tobiska L (2005) Equilibrium shapes of a ferrofluid drop. Proceedings in applied mathematics and mechanics, vol 5. Wiley Online Library, pp 837–838
16. Bhattacharjee D, Atta A (2022) Topology optimization of a packed bed microreactor involving pressure driven non-Newtonian fluids. React Chem Eng 7(3):609–618
17. Bhattacharjee D, Chakraborty S, Atta A (2022) Passive droplet sorting engendered by emulsion flow in constricted and parallel microchannels. Chem Eng Process Process Intensif 181:109126
18. Md Hassan R, Zhang J, Wang C (2018) Deformation of a ferrofluid droplet in simple shear flows under uniform magnetic fields. Phys Fluids 30(9):092002
19. Santra S, Mandal S, Chakraborty S (2018) Electrohydrodynamics of confined two-dimensional liquid droplets in uniform electric field. Phys Fluids 30(6):062003

20. Mandal S, Ghosh U, Bandopadhyay A, Chakraborty S (2015) Electroosmosis of superimposed fluids in the presence of modulated charged surfaces in narrow confinements. J Fluid Mech 776:390–429
21. Stone HA, Leal LG (1989) Relaxation and breakup of an initially extended drop in an otherwise quiescent fluid. J Fluid Mech 198:399–427
22. Ghaffari A, Hashemabadi SH, Bazmi M (2015) Cfd simulation of equilibrium shape and coalescence of ferrofluid droplets subjected to uniform magnetic field. Colloids Surf, A 481:186–198